# Evaluation of jitter vibration-induced image interpretability degradation for remote sensing data using GIQE



# Evaluation of jitter vibration-induced image interpretability degradation for remote sensing data using GIQE

**M A Ali[1], A Omer[2], F Eltohamy[1], M Hanafy[1]**

[1] Electrical Engineering Department, Military Technical College, Cairo, Egypt
[2] Mechanical Engineering Department, Military Technical College, Cairo, Egypt

E-mail: mohamed.ahmed.ali@yandex.com

**Abstract.** Remote sensing data plays an important role in various military and civilian applications. The quality of remote sensing data is the key to the success of these applications. remote sensing data are subjected to a variety of distortions from different sources, including acquisition, onboard compression, transmission, on-ground processing, and satellite vibrations. These distortions cause a great loss of image quality. In this paper, jitter vibration is modeled according to the modulation transfer function (MTF). Jitter-induced degradation is evaluated in terms of the National Imagery Interpretability Rating Scale (NIIRS), which is measured in terms of the general image quality equation (GIQE). A study on the third, fourth, and fifth versions of the GIQE is made using a remote sensing data set to select the appropriate version that could be used in evaluating the amount of jitter-induced degradation. The key result of this paper is that the fourth version of the GIQE is the most proper one in evaluating the amount of jitter-induced degradation.

## 1. Introduction

Satellite micro-vibration is a significant problem that degrades the quality of remote sensing data and hence diminishes the amount of information that can be extracted. Several attempts have been conducted to classify the satellite vibrations and to study their effect on satellite image degradation [1, 2]. There are many sources of satellite vibrations like rotary mechanisms such as Reaction Wheel Assemblies, and other satellite sub-systems (propulsion, structure, thermal control, power, communication, optical lens shutter, and electrical noise) [3]. Many satellites, like the Chinese satellite ZiYuan-3, the Japanese Advanced Land Observing Satellite (ALOS), and the French satellite Pleiades, exhibit jitter vibration. This vibration is a significant factor in the deterioration of satellite image quality [4]. The NIIRS is a ten-level metric that describes the interpretability of images numbered from 0 to 9, where level zero indicates the worst interpretability and level nine corresponds to the best quality [5, 6]. GIQE was proposed to relate the technical image quality measures, such as (MTF), Ground Sampling Distance (GSD), and Signal to Noise Ratio (SNR), to application image quality measures such as NIIRS. GIQE estimates NIIRS as a function of GSD, SNR, Relative Edge Response (RER), Sharpening Filter Gain (G), and Edge Overshoot (H) [6]. Five versions of the GIQE are proposed. The first and second versions are not declared and are used as classified data. The third version is released in 1994, it was used mainly with aerial and satellite images. The fourth version was published in 1997, it was used for satellite images. The fifth version of the GIQE was published by Harrington in 2015 [7]. A few studies have been carried out to find the effect of some degradation parameters on the NIIRS, Hua-mei Chen et el. (2016) investigated the effect of image compression on NIIRS rating degradation using automated image analysis [8], and Erik Blasch et el. (2018) suggested

a methodology to predict compression-induced image interpretability degradation [9]. In this paper, the MTF of a model of an image degraded by jitter vibration is proposed. Also, a model of the micro-vibration-induced information distortion in terms of NIIRS is discussed. A study on three versions of the GIQE, using three different GeoEye-1 images, is introduced to examine the change in the image interpretability due to five different levels of jitter vibration. The rest of this paper is organized as follows: Section 2 introduces jitter vibration. Section 3 is an overview of the versions of GIQE and their main effective parameters. Section 4 illustrates the approaches used to evaluate the reduction in NIIRS due to jitter vibration. Finally, the conclusion is presented in section 5.

## 2. Jitter vibration

A small, quick, and irregular variation or fluctuation is referred to as jitter, and it typically pertains to digital communications like audio or video streams. In other words, jitter is a signal's departure from its typical time. In data transmission, audio and video processing, and other fields where exact timing is important, a jitter can lead to signal distortion or degradation [10].

Contrarily, vibration describes an object's oscillatory motion about a fixed point or axis. Mechanical imbalances, outside influences, or electrical interference are just a few of the causes. A vibration's magnitude, frequency, and direction can all be determined. Inconvenience or damage to machines can result from excessive vibration [10].

Jitter vibration originates from dynamic mechanical disturbances, attitude control operation, thermal change, and other impacting factors [10]. Jitter vibration is a random movement where the image oscillates during the integration time. According to the central limit theorem jitter vibration can be modeled by Gaussian distribution [11]. Hence, the MTF of jitter vibration, $MTF_{jitter}$, is given by:

$$MTF_{jitter} = e^{-2\pi^2\sigma^2N^2} \tag{1}$$

Where σ is the root mean square random displacement [m], and N is the spatial frequency [$m^{-1}$]. The value of σ controls the amount of jitter vibration. The increase of σ leads to a considerable influence of jitter vibration on image quality. The value of σ is related to the detector array size of the satellite camera. When σ is about the limits of 10% of the detector array size then the effect of the jitter vibration on the image quality is not significant. The insignificant effect is due to the system MTF characteristics in this case [11]. The term detector array size refers to the size of the image sensor, which has an impact on the image's resolution and field of view [10, 11].

## 3. General Image Quality Equation (GIQE)

NIIRS is an image quality metric used to indicate the amount of information that can be extracted from satellite images [5]. GIQE was proposed to relate the technical quality measures, including GSD, MTF, and SNR, to quality measures such as NIIRS [5, 7, 12, 13]. There are three versions of the GIQE as follows [7]:

$$GIQE_3 = [6.514 - 3.32\times\log_{10}(GSD) + 3.32\times\log_{10}(RER) - 1.48\,(H) - G/SNR] \tag{2}$$

$$GIQE_4 = [5.21 - a\times\log_{10}(GSD) + b\times\log_{10}(RER) - 0.656\,(H) - 0.344\,(G/SNR)] \tag{3}$$

Where the selection of the coefficients *a* and *b* are set according to the value of RER; for RER< 0.9, a = 3.16 and b = 2.817, and for RER ≥ 0.9, a = 3.32 and b = 1.559.

$$GIQE_5 = [4.274 - 3.32\times\log_{10}(GSD) + [3.32[1-\exp(-1.9/SNR)] \times \log_{10}(RER)] - 2[\log10(RER)]^4 - 1.8/SNR] \tag{4}$$

### *3.1. Ground Sampling Distance (GSD)*

The GSD is the main parameter for calculating the GIQE and contributes to more than 70% of the total value of the GIQE [14]:

$$GSD = h\,x\,/\,f \tag{5}$$

Where h is the satellite altitude [km], f is the camera focal length [m], and x is the detector pixel cell size [μm].

*3.2. Signal to Noise Ratio (SNR)*

The signal-to-noise ratio (SNR) parameter covers noise originating from many imaging systems sources, such as detector-based sources (dark current, read noise, photon, and quantization noise), and noise originates due to atmospheric influences and other sources [5]. The SNR is one of the elements of the image quality that characterizes the radiometric resolution. The image noise quantifies the variation of the radiances at a given radiance level for a uniform landscape. SNR is given by [14]:

$$SNR = \mu\,/\,std \tag{6}$$

Where μ is the mean of a series of radiances for a uniform landscape and std is the standard deviation of this series.

*3.3. Relative Edge Response (RER)*

RER measures the image sharpness and can be calculated by three different techniques: the slanted-edge method, the partial-reference technique, and the no-reference technique [15]. In the no-reference technique four various metrics, including Blind blur (BM), Edge Intensity (EI), Perceptual RER (PRER), and Frequency Ratio (FR), are calculated to estimate the RER value as follows [15]:

$$RER(BM) = 1.17 - (1.15\times BM) \tag{7}$$
$$RER(EI) = -0.28 + 1.3 \times (EI/100)^{(1/4)} \tag{8}$$
$$RER(PRER) = 0.10 + (0.55\times PRER) \tag{9}$$
$$RER(FR) = -0.26 + 3\times(FR)^{(1/4)} \tag{10}$$

And the RER is the average value of the calculated RERs given in equations (7-10) as follows:

$$RER=[RER(BM) + RER(EI) + RER(PRER) + RER(FR)] / 4 \tag{11}$$

*3.4. Height Overshoot (H)*

Both versions $GIQE_3$ and $GIQE_4$ consider the height overshoot, H, in their calculations. A method for computing, edge overshoot from an edge response profile is as follows: first, from the edge center, 0 image pixel, detect three adjacent image pixels in both left and right directions, -3 to +3 image pixels, and obtain the normalized edge profile. Referring to Figure 1, for an edge response greater than 1 (case 1), the maximum edge response value of the normalized edge profile between +1 to +3 pixels is selected as the H value. Whereas, for an edge response less than 1 (case 2), the edge response corresponding to +1.25 pixels is selected as the H value [7].

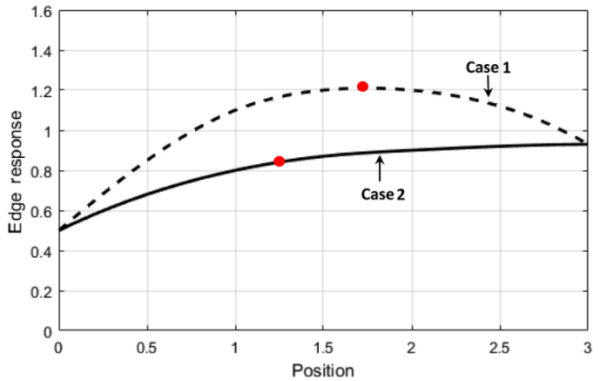


**Figure 1.** Edge overshoot calculations [7]

*3.5. Sharpening Filter Gain*

Sharpening filter gain, G, can be calculated from the coefficients of the correction kernel, w, where G is given by [7, 9]:

$$G= \frac{\sqrt{\sum_{(m,n)} w_{m,n}^2}}{\sum_{(m,n)} w_{m,n}} \quad (12)$$

Where m and n represent the pixels of the kernel. The raw image is characterized by a sharpening filter gain G = 1 [9].

## 4. Estimating NIIRS loss approaches

In this paper, two approaches are used to estimate NIIRS degradation due to jitter vibration. The first approach is as follows:

Step 1: Using three different images from the GeoEye-1 satellite.

Step 2: Calculating GSD given in eq. (5) for the GeoEye-1 satellite images.

Step 3: Calculating the detector array size, X [16]:

$$X = \frac{(x \times SW)}{GSD} \quad (13)$$

Where SW is the swath width [km].

Step 4: Applying the Jitter vibration effect on the three GeoEye-1 images using $MTF_{jitter}$, given in eq. (1), for σ =10, 50,100,150, and 200 % of X.

Step 5: Using the steps that have been discussed in the previous section to calculate SNR, G, H, and RER values for each image.

Step 6: Calculate NIIRS using the different versions given in equations (2, 3, and 4).

Samuel T Thurman and James R Fienup concluded that when applying the GIQE on aberrated images it is better to drop the H term in both versions $GIQE_3$ and $GIQE_4$ to reach results closest to reality [13]. So that the second approach will conclude the previous six steps, except for calculating the H values. In this case, the term H will be dropped totally from the GIQE. The equation is repeated for versions 3 and 4 only because version 5 did not have the term H or even G.

## 5. Comparative study

Our investigation considers the degrading effect of jitter vibration on the GeoEye-1 satellite images. GeoEye-1 has the following specifications [17]:

**Table 1.** Specifications of GeoEye-1 satellite camera**.**

| Parameter | Value |
|---|---|
| Spatial resolution (GSD) | 0.41 [m] |
| Detector pixel cell Size (x) | 8 [μm] |
| Orbital height (h) | 681 [km] |
| Camera focal length (f) | 13.3 [m] |
| Aperture diameter (D) | 1.1 [m] |
| Swath width (SW) | 15.2 [km] |
| Integration time | 54.4 [μsec] |

The selected three images are given in Figure (2). They are as follows:
Image-1 is of size (512 X 512) pixels, the area of Kauai Island, Hawaii, USA.
Image-2 is of size (512 X 512) pixels, the area of Ferrari World, Dubai, UAE.
Image-3 is of size (512 X 512) pixels, the area of Boston, Massachusetts, USA.

From table (1) and using equation (13), the detector array size X is equal to 29.96 [cm]. Figure (3) represents normalized $MTF_{jitter}$ for different values of σ = 10, 50,100,150, and 200% of the calculated detector array size, X.

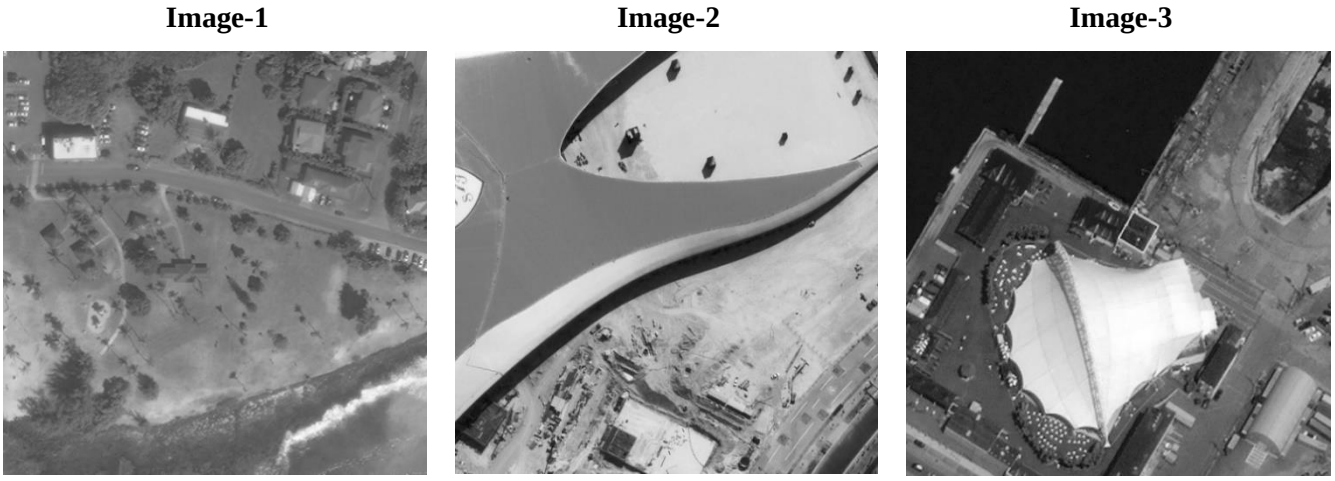


**Figure 2.** Selected data set of GeoEye-1 satellite images.

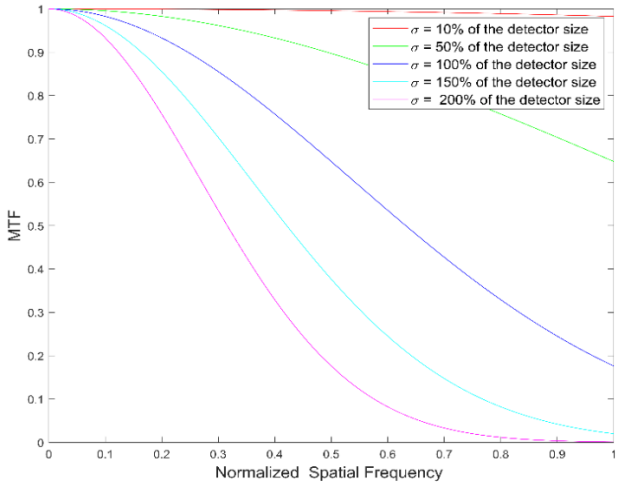


**Figure 3.** Jitter MTF curves for different values of σ.

The obtained images after applying the Jitter effect, for different values of σ, are shown in figures 4, 5, and 6.

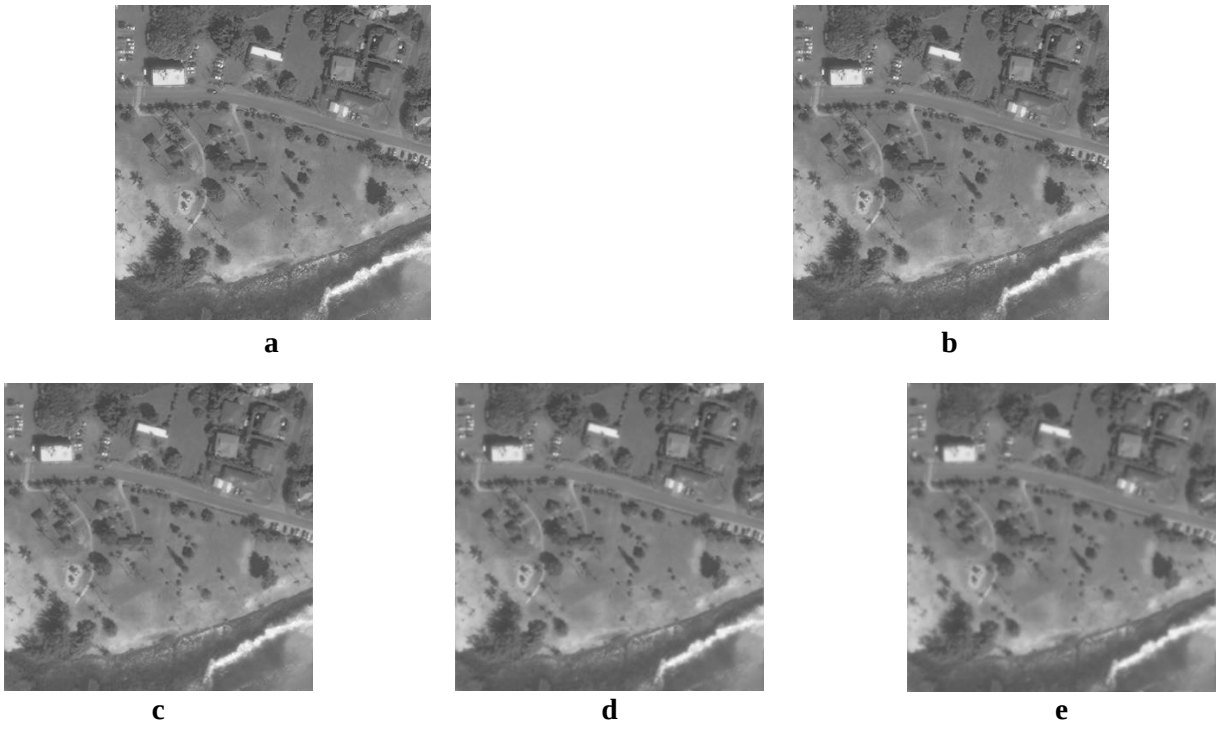

**Figure 4.** The corresponding degraded images for image-1: (a) σ = 0.1X, (b) σ = 0.5X, (c) σ = X, (d) σ = 1.5X, (e) σ = 2X.

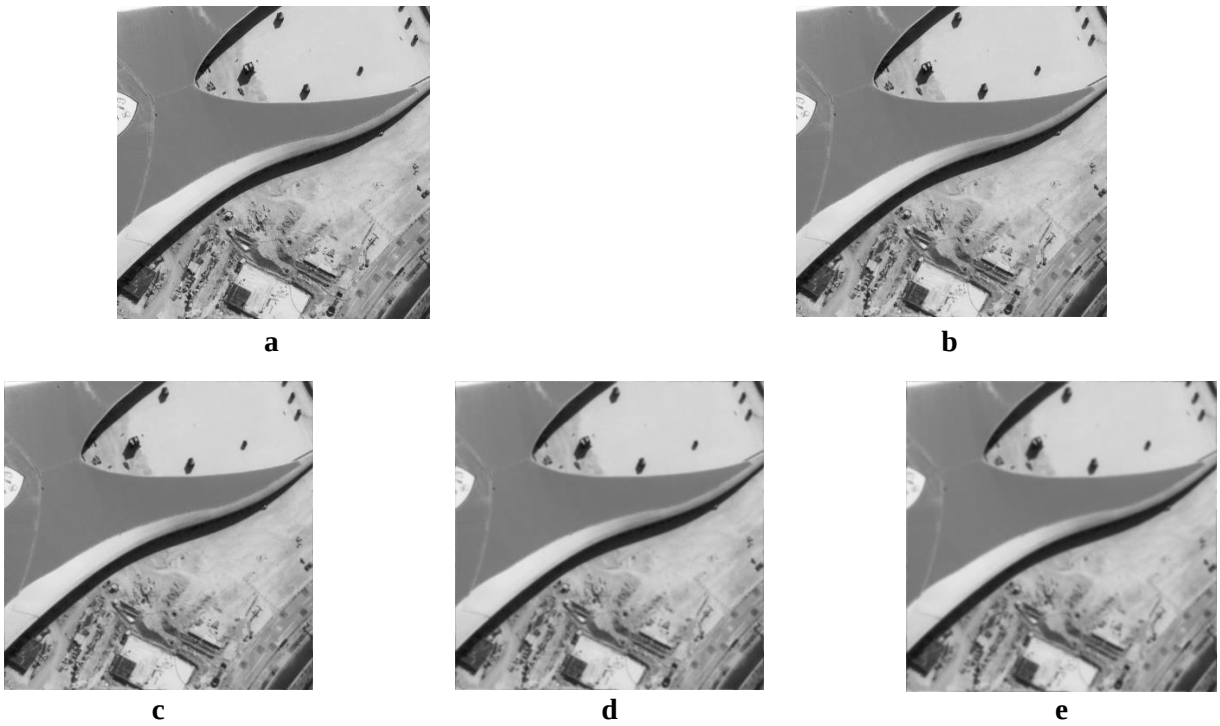

**Figure 5.** The corresponding degraded images for image-2: (a) σ = 0.1X, (b) σ = 0.5X, (c) σ = X, (d) σ = 1.5X, (e) σ = 2X.

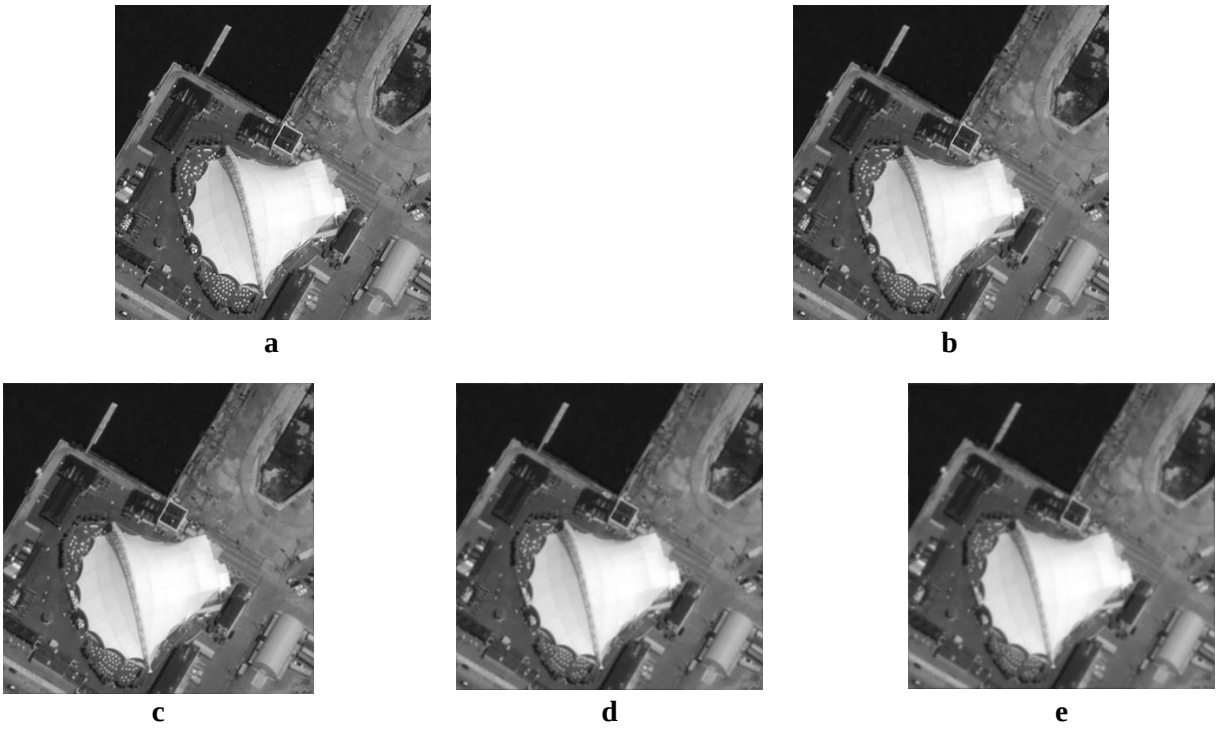


**Figure 6.** The corresponding degraded images for image-3: (a) σ = 0.1X, (b) σ = 0.5X, (c) σ = X, (d) σ = 1.5X, (e) σ = 2X.

The SNR calculations for all cases of the three images illustrated above are listed in table (2) as follows:

**Table 2.** Calculated SNR.

| | **Original** | **σ = 0.1X** | **σ = 0.5X** | **σ = X** | **σ = 1.5X** | **σ = 2X** |
|---|---|---|---|---|---|---|
| Image-1 | 20.99 | 20.99 | 20.46 | 19.49 | 19.20 | 18.91 |
| Image-2 | 16.15 | 16.15 | 16.03 | 15.9 | 15.8 | 15.8 |
| Image-3 | 13.8 | 13.8 | 13.8 | 13.6 | 13.44 | 13.4 |

Then we calculate the sharpening filter gain, G, knowing that G is not changing in each image because it is a sensor-related parameter [8]. Table 3 represents the G results according to changes in the σ parameter.

**Table 3.** Calculated sharpening filter gain, G.

| **Image** | **G** |
|---|---|
| Original | 1 |
| σ = 0.1X | 1.0010 |
| σ = 0.5X | 1.4441 |
| σ = X | 3.1115 |
| σ = 1.5X | 4.6714 |
| σ = 2X | 6.2286 |

The overshoot parameter, H, is calculated for each image in both horizontal and vertical directions, then the H is the geometric mean of both directions' values. Table 4 represents calculated H values for each degraded image.

**Table 4.** Calculated overshoot parameter, H.

| | **Original** | **σ = 0.1X** | **σ = 0.5X** | **σ = X** | **σ = 1.5X** | **σ = 2X** |
|---|---|---|---|---|---|---|
| Image-1 | 0.8928 | 0.8502 | 0.7133 | 0.6841 | 0.6759 | 0.6759 |
| Image-2 | 0.7820 | 0.78 | 0.7648 | 0.7494 | 0.6937 | 0.6902 |
| Image-3 | 0.5722 | 0.5722 | 0.5506 | 0.5006 | 0.3940 | 0.3377 |

The values of the overshoot in all cases are less than one. The overshoot value decrease as the jitter effect increases. Equations from 7 to 11 are used to calculate the RER values for each image. Tables (5), (6), and (7) list the RER values for images-1, image-2, and image-3 respectively.

**Table 5.** Calculated RERs for image-1.

| | **BM** | **EI** | **FR** | **PRER** | **RER** |
|---|---|---|---|---|---|
| Original | 0.8989 | 0.6095 | 0.4234 | 0.3262 | 0.5645 |
| σ = 0.1X | 0.8987 | 0.6095 | 0.4233 | 0.3261 | 0.5644 |
| σ = 0.5X | 0.8443 | 0.5847 | 0.3473 | 0.3255 | 0.52545 |
| σ = X | 0.7006 | 0.5298 | 0.2023 | 0.3233 | 0.439 |
| σ = 1.5X | 0.5824 | 0.4889 | 0.1262 | 0.3198 | 0.379325 |
| σ = 2X | 0.4880 | 0.4584 | 0.0973 | 0.3151 | 0.3397 |

**Table 6.** Calculated RERs for image-2**.**

| | **BM** | **EI** | **FR** | **PRER** | **RER** |
|---|---|---|---|---|---|
| Original | 0.8346 | 0.6284 | 0.4667 | 0.3225 | 0.56305 |
| σ = 0.1X | 0.8345 | 0.6284 | 0.4667 | 0.3226 | 0.56305 |
| σ = 0.5X | 0.7872 | 0.6078 | 0.3975 | 0.3221 | 0.52865 |
| σ = X | 0.6517 | 0.5633 | 0.2584 | 0.3198 | 0.4483 |
| σ = 1.5X | 0.5301 | 0.5296 | 0.1826 | 0.3166 | 0.389725 |
| σ = 2X | 0.4339 | 0.5041 | 0.1541 | 0.3125 | 0.35115 |

**Table 7.** Calculated RERs for image-3.

| | **BM** | **EI** | **FR** | **PRER** | **RER** |
|---|---|---|---|---|---|
| Original | 0.8137 | 0.6439 | 0.5113 | 0.3076 | 0.5691 |
| σ = 0.1X | 0.8135 | 0.6440 | 0.5115 | 0.3077 | 0.5691 |
| σ = 0.5X | 0.7822 | 0.6245 | 0.4741 | 0.3071 | 0.546975 |
| σ = X | 0.6908 | 0.5772 | 0.3936 | 0.3054 | 0.49175 |
| σ = 1.5X | 0.5843 | 0.5345 | 0.3490 | 0.3027 | 0.442625 |
| σ = 2X | 0.4884 | 0.5009 | 0.3339 | 0.2991 | 0.405575 |

In general, RER values decrease as the influence of jitter vibration increases. Using the values of the basic parameters of the GIQE, including SNR, G, H, and RER, which are listed in tables (2-7). applying these values in equations (2-4) are corresponding to the three different versions of the GIQE. Tables (8-10) list the calculated values of the NIIRS versions 3, 4, and 5 respectively for the original non-degraded image and the jitter-degraded images.

**Table 8.** Calculated NIIRS for the third version of GIQE.

| | **Original** | **σ = 0.1X** | **σ = 0.5X** | **σ = X** | **σ = 1.5X** | **σ = 2X** |
|---|---|---|---|---|---|---|
| Image-1 | 5.6 | 5.66 | 5.74 | 5.44 | 5.15 | 4.91 |
| Image-2 | 5.72 | 5.73 | 5.63 | 5.31 | 5.09 | 4.85 |
| Image-3 | 6.06 | 6.06 | 6.01 | 5.80 | 5.69 | 5.53 |
| Average | 5.8 | 5.8 | 5.8 | 5.51 | 5.31 | 5.09 |

**Table 9.** Calculated NIIRS for the fourth version of GIQE.

| | **Original** | **σ = 0.1X** | **σ = 0.5X** | **σ = X** | **σ = 1.5X** | **σ = 2X** |
|---|---|---|---|---|---|---|
| Image-1 | 5.13 | 5.15 | 5.15 | 4.92 | 4.72 | 4.39 |
| Image-2 | 5.19 | 5.19 | 5.12 | 4.89 | 4.72 | 4.56 |
| Image-3 | 5.34 | 5.34 | 5.29 | 5.15 | 5.05 | 4.95 |
| Average | 5.22 | 5.22 | 5.18 | 4.98 | 4.83 | 4.63 |

**Table 10.** Calculated NIIRS for the fifth version of GIQE.

| | **Original** | **σ = 0.1X** | **σ = 0.5X** | **σ = X** | **σ = 1.5X** | **σ = 2X** |
|---|---|---|---|---|---|---|
| Image-1 | 5.39 | 5.39 | 5.37 | 5.32 | 5.27 | 5.21 |
| Image-2 | 5.34 | 5.34 | 5.33 | 5.28 | 5.23 | 5.18 |
| Image-3 | 5.31 | 5.31 | 5.30 | 5.27 | 5.23 | 5.20 |
| Average | 5.35 | 5.34 | 5.33 | 5.29 | 5.24 | 5.20 |

From the results obtained in tables (8-10), we conclude the following:

- In general, for each image as the value of σ increases the values of the NIIRS decrease. Considering the third version of GIQE, some results, especially for σ <= 50% of the detector array size, violate this rule. This may be attributed to the high weight given to the overshoot factor, H=1.48, and accordingly, the gradual decrement in the overshot factor cannot compensate for this difference. These results confirm the conclusion given in [13] which states that it is better to drop the H term in both versions 3 and 4 to reach results closest to reality. This problem appears to a less effect in the fourth version because the weight of the overshoot factor H is reduced, H=0.656. However, the same problem does not appear in the fifth version of GIQE because the overshoot factor H is already dropped.
- The average difference of NIIRS for the third and fourth versions of GIQE, from the original image to the case of σ = 200% of the detector array size, ΔNIIRS = 0.71 and 0.59, respectively. Whereas, for the fifth version ΔNIIRS = 0.15 indicating the incapability to sense the occurrence of degradation due to jitter vibration.

The second approach is used to eliminate the effect of the H parameter on the overall results of the third and fourth versions of GIQE to estimate the interpretability of the degraded image calculations. Tables (11, and 12) represent the results of the GIQE after dropping the H parameter from the NIIRS calculations.

**Table 11.** Calculated NIIRS for the third version of GIQE after dropping the H parameter.

| | **Original** | **σ = 0.1X** | **σ = 0.5X** | **σ = X** | **σ = 1.5X** | **σ = 2X** |
|---|---|---|---|---|---|---|
| Image-1 | 6.92 | 6.85 | 6.8 | 6.45 | 6.15 | 5.91 |
| Image-2 | 6.89 | 6.88 | 6.76 | 6.42 | 6.12 | 5.87 |
| Image-3 | 6.9 | 6.9 | 6.82 | 6.54 | 6.27 | 6.03 |
| Average | 6.9 | 6.87 | 6.79 | 6.47 | 6.18 | 5.93 |

**Table 12.** Calculated NIIRS for the fourth version of GIQE after dropping the H parameter.

| | **Original** | **σ = 0.1X** | **σ = 0.5X** | **σ = X** | **σ = 1.5X** | **σ = 2X** |
|---|---|---|---|---|---|---|
| Image-1 | 5.71 | 5.71 | 5.62 | 5.37 | 5.16 | 4.84 |
| Image-2 | 5.71 | 5.71 | 5.62 | 5.38 | 5.18 | 5.02 |
| Image-3 | 5.71 | 5.71 | 5.66 | 5.48 | 5.31 | 5.17 |
| Average | 5.71 | 5.71 | 5.63 | 5.41 | 5.21 | 5.01 |

From tables (11, and 12), we conclude that upon increased σ values, the calculated NIIRS values decrease. The NIIRS values produced a notable increment in the final obtained results by a value greater than 1 for the third version of GIQE, and by a value greater than 0.3 for the fourth version of GIQE.

The results obtained from the previous analysis are summarized in figure (7) and then compared with the typical NIIRS value of 5.3 for the GeoEye-1 satellite original images, which is represented by the horizontal red line [17]. Calculating the NIIRS values without taking into consideration the H parameter gives a result very far and higher than the typical value stated in [17].

From figure (7) we can conclude that NIIRS 5 gives a result close to the typical value of the GeoEye-1 NIIRS when used with the original images only.

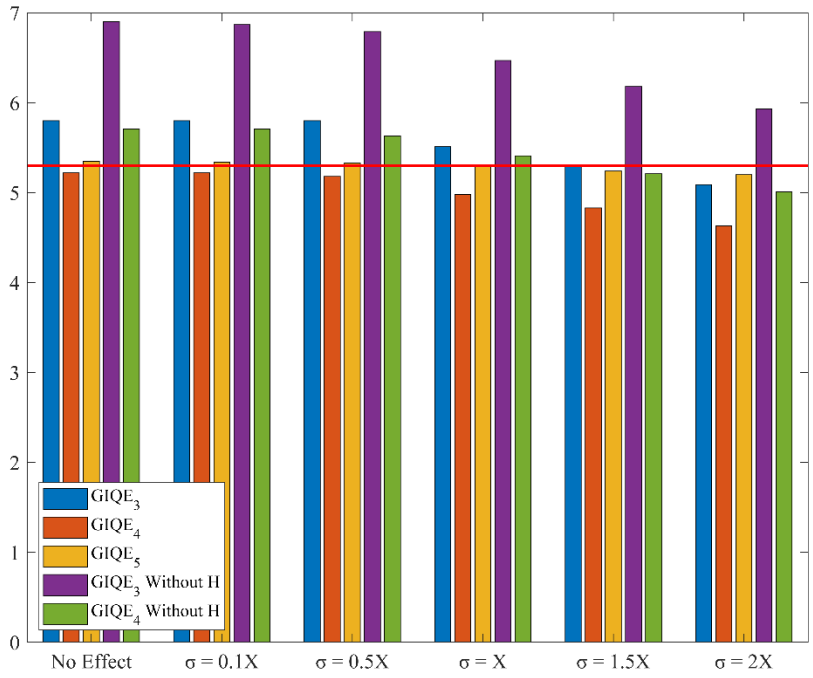


**Figure 7.** Summarization of all versions of the GIQE average values.

## 6. Conclusion

This paper presents the effects of Jitter vibration on the quality of remote-sensing satellite images in terms of image interpretability. This paper studied the decrement in the NIIRS due to the five different levels of jitter vibration using three different versions $GIQE_3$, $GIQE_4$, and $GIQE_5$. This study has shown that the $GIQE_4$ is the most suitable to describe the degradation caused by the jitter vibration. This investigation suggests that $GIQE_5$ can be used only in case of no degradation occurred, as shown in figure 7. Eliminating the H parameter from $GIQE_3$, and $GIQE_4$ enhances the ability of the GIQE to sense the gradual degradation that occurred due to jitter vibration. Therefore, as σ increases the values of the GIQE decrease. But eliminating the H parameter leads to higher values of NIIRS than the typical values mentioned in the GeoEye-1 data sheet, as shown in figure 7.

## References

[1] Wulich D and Kopeika N 1987 *Optical Engineering* **26** 529–533
[2] Haghshenas J 2015 *SPIE Proceedings* **9626** 96262P-1
[3] Addari D and Aglietti G S 2016 *A semi-empirical approach for the modelling and analysis of microvibration sources on-board* spacecraft PhD thesis
[4] Ye Z, Xu Y, Zheng S, Tong X, Xu X, Liu S, Xie H, Liu S, Wei C and Stilla U 2020 Resolving time-varying attitude jitter of an optical remote sensing satellite based on a time-frequency analysis *Optics Express* **28** 15805
[5] Wong S and Jassemi R 2014 (Ottawa: Defence Research and Development Canada)
[6] Irvine and John M 1997 National imagery interpretability rating scales (NIIRS): overview and methodology *SPIE Proceedings*
[7] Valenzuela A Q and Reyes J C 2019 Comparative study of the different versions of the general image quality equation *ISPRS Annals of the Photogrammetry, Remote Sensing and Spatial Information Sciences* **IV-2/W5** 493–500
[8] Chen H M, Blasch E, Pham K, Wang Z and Chen G 2016 An investigation of image compression on NIIRS rating degradation through automated image analysis *SPIE Proceedings*
[9] Blasch E, Chen H M, Irvine J M, Wang Z, Chen G, Nagy J and Scott S 2018 Prediction of compression-induced image interpretability degradation *Optical Engineering* **57** 1
[10] Chao F, Yitao L and Aihong G 2009 Influence Analysis of jitter on image quality of Remote Sensing Camera *2009 International Conference on Environmental Science and Information Application Technology* 461–464
[11] Holst G C 2000 *CCD arrays, cameras, and displays* (Bellingham, WA: SPIE Optical Engineering Press)
[12] Hoffman C 2016 *Encyclopedia of optical and photonic engineering* (Boca Raton: CRC Press)
[13] Thurman S T and Fienup J R 2010 Application of the general image-quality equation to aberrated imagery *Applied Optics* **49** 2132
[14] Li L, Luo H and Zhu H 2014 Estimation of the image interpretability of ZY-3 sensor corrected Panchromatic Nadir Data *Remote Sensing* **6** 4409–29
[15] Young D L 2014 Video interpretability and quality estimation
[16] Sun Y, Rao P and Hu T 2021 Parameter design and performance evaluation of a large-swath and high-resolution space camera *Sensors* **21** 4106
[17] Mohamed A, Eltohamy F and Gouda I 2016 Estimation of NIIRS for high resolution satellite images, using the simplified GIQE *International Journal of Innovative Research in Computer and Communication Engineering* **4** 8403–08